Available online at www.sciencedirect.com
SCIENCE DIRECT
Polymer 47 (2006) 3410–3425
polymer
www.elsevier.com/locate/polymer

Molecular changes on drawing isotopic blends of polyethylene and ethylene copolymers. Part 2. MCIRS studies

Sandry Coutry, Stephen J. Spells *

Materials and Engineering Research Institute, Sheffield Hallam University, City Campus, Sheffield S1 1WB, UK

Received 8 September 2005; received in revised form 9 January 2006; accepted 13 March 2006
Available online 11 April 2006

Abstract

The technique of mixed crystal FTIR spectroscopy has been applied to uniaxially drawn isotopic blends of linear polyethylene and ethylene copolymers. Following the drawing of melt-quenched samples at 1 mm min^{-1}, clamped samples were cooled with liquid nitrogen. Analysis of the CD_2 bending vibration of the 'guest' perdeuterated species enabled the arrangement of crystal stems to be characterised. Changes in band components observed were identified with the processes of polymer crystallisation, the untwisting of lamellar ribbons perpendicular to the draw direction and coarse slip. For example, the appearance of new doublets or increased splittings is related to crystallisation, while an increase in singlet band area, at least at higher draw ratios, is indicative of coarse slip. Crystallisation appears to be complete at a draw ratio of 4 for a linear polyethylene sample with low guest molecular weight. For similar copolymer 'guest' molecular weights, the processes identified above are delayed to higher levels of deformation. This was attributed to copolymer branches hindering both crystallisation and chain translation through lamellae. Estimates of the crystallite block size present after drawing enable a quantitative description of coarse slip to be obtained. A progressive increase in width of the central singlet for two of these samples is tentatively ascribed to variations in molecular strain.

Keywords: Drawing; FTIR; Polyethylene

1. Introduction

The uniaxial deformation of polyethylene (PE) is a complex process, with molecular form playing a major role in determining the evolution of structure (see, for example, Ref. [1]). Recent time-resolved X-ray studies [2–4] have enabled structural changes to be documented simultaneously with load/extension data. This provides direct information on structure/property relationships. Nevertheless, the structural information obtained is primarily at the level of the crystalline lamellae, rather than that of individual molecules. The evolution of molecular conformation with drawing is still poorly understood.

The current work is part of a wider study of well-characterised, metallocene-catalysed polymers, involving a combination of small angle neutron scattering (SANS) and infra-red spectroscopic measurements. Both techniques rely on the use of isotopic (deuterium) labelling of a small proportion (3–5%) of 'guest' molecules within an unlabelled matrix. The aim is to characterise the changes in molecular conformation in melt quenched films with drawing. A previous part, concerned with the SANS measurements, has shown that copolymer guest molecules (with either butyl or hexyl branches) in either copolymer or linear matrix show no significant departures from affine behaviour for draw ratios up to around 3 [5]. Conversely, linear guest molecules showed deviations at draw ratios as low as 1.5, prompting the question of whether this difference relates to a delay in some of the various crystal deformation processes in the former case. Such behaviour has been suggested elsewhere [3]. Infra-red dichroism measurements on isotactic polypropylene indicate that the amorphous component deforms in an affine manner, with crystallites causing early departures from affine behaviour [6]. Our SANS measurements were similarly interpreted as indicating a delay in crystallite disruption for copolymer guest molecules.

The use of mixed crystal infra-red spectroscopy (MCIRS) to study chain conformation in isotopic blends of PE has been reviewed elsewhere [7]. Only the key points will be reiterated here. In essence, the technique makes use of the IR CD_2 bending vibration to determine the shape and size of groups of deuterated crystal stems (each corresponding to a single traverse of the crystal). The CD_2 bending vibration appears

* Corresponding author. Tel.: +44 114 225 3428; fax: +44 114 225 3501.
E-mail address: s.j.spells@shu.ac.uk (S.J. Spells).

0032-3861/$ - see front matter © 2006 Elsevier Ltd. All rights reserved.
doi:10.1016/j.polymer.2006.03.041

as a singlet if all deuterated stems are isolated from similar nearest neighbours in ⟨110⟩ directions. Groups of deuterated stems having similar nearest neighbours contribute doublet components to the spectrum. The magnitude of the doublet splitting depends primarily on the size, but to some extent also on the shape, of these groups. FTIR measurements are made on samples cooled to around −173 °C, in order to maximise the doublet splittings.

The application of MCIRS to melt-crystallised PE, the starting material for this work, has also been considered previously [8]. In relation to studies of deformation, the technique has been applied to rolled single crystal mats of PE [9]. Here the initial groups of labelled stems are large, and there is a significant reduction in their size with rolling. This indicates the extent of disruption of the crystallites: in this way the lateral size of blocks detached from the original crystals was estimated to have reached around 36 Å for a roll ratio of 6.0. With regard to uniaxial deformation of melt crystallised PE, isotopic blends have been used to study the development of orientation functions for IR bands arising from both labelled and unlabelled molecules [10]. No dependence on isotope was noted in the evolution of orientation functions, although some differences were found for the case of biaxial stretching.

The range of processes which occur during polymer deformation—including fine and coarse slip, twinning, Martensitic transformation, lamellar untwisting, rotation and separation—have been widely studied, but spectroscopic techniques in general and MCIRS in particular have the capability of providing a unique molecular insight. The break-up of crystallites by coarse slip, for example, can be followed through changes in the size of groups of labelled chains. In this work we report such measurements on the uniaxial deformation of blends of linear polymers and of ethylene copolymers.

The increasing commercial use of ethylene copolymers and their importance in influencing the drawing behaviour of products demonstrates the value of studying copolymer materials alongside linear polymers. In this work, copolymers with controlled homogeneous branch contents are used, with molecular weights matched to those of the linear polymers studied. The aim of this work is to identify any differences in the evolution of molecular conformation with drawing and in the stages of deformation listed above.

Two particular features of copolymer structure and mechanical behaviour should be mentioned here. First, the critical strain required for the onset of fibrillation during drawing undergoes a step change in the region of molecular weight 150,000–200,000 [11]. Although the molecular weight of the guest deuterated copolymer in both such samples considered here was below this region, deformation behaviour must primarily be related to the matrix material in the isotopic blends.

Secondly, double melting peaks in DSC experiments on similar polyethylene copolymers [12] have been interpreted in terms of two-crystal populations, one of which has undergone some rearrangement of the crystal/amorphous interface [13]. There are indications of double melting peaks in our copolymer samples [14], although they are not at all clearly resolved as is the case for isothermal crystallisation [12]. For this reason, we have not considered the deformation of two distinct crystal populations in our analysis here.

2. Spherulite deformation and MCIRS spectra

The deformation of spherulites has been studied by a range of techniques over many years. Direct observations of deformation in spherulitic LDPE films, using optical microscopy, showed the response of spherulites to be non-uniform and highly recoverable [15]. Importantly, spherulite radii perpendicular to the draw direction were found to be initially affected by deformation, while at higher draw ratios the whole spherulite became deformed, giving rise to a fibre morphology. Models of spherulite deformation have largely envisaged affine deformation of the spherulite superstructure, followed by crystallite rearrangement [16]. A modification of this type of model considered the effects of tie chains linking adjacent lamellae [17,18]. These resulted in the tilting of the crystal *c*-axis within the lamellae in the polar zones of spherulites, with the untwisting of lamellae in the equatorial zone.

In order to interpret FTIR spectra of drawn spherulitic films, it is necessary to consider the possible changes in the local unit cell orientation. While drawing changes the initial spherulitic morphology with the *b*-axis radial to a fibre morphology with *c* aligned with the draw direction, the moderate draw ratios achieved in this work do not produce a fibre orientation, so we are generally dealing with an intermediate situation. We make the assumption here that lamellar segments rotate in order to move the local *c*-axis towards the draw direction. The arrangements for both the undeformed spherulite and its deformed analogue are shown schematically in Fig. 1.

We consider first radii perpendicular to the draw direction and in the sample plane, at the two points $1_\perp$ and $2_\perp$. In the region $1_\perp$, the *c*-axis is already aligned with the draw direction in the undeformed spherulite and is thus unaffected by deformation. In the region $2_\perp$, with the *c*-axis perpendicular to the sample plane, a rotation about the local *b*-axis would move the *c*-axis towards the draw direction: the *a*-axis leaves the plane of the sample, while the *c*-axis moves into that plane (Fig. 1(b)). For intermediate positions between $2_\perp$ and $1_\perp$, a similar mechanism would be envisaged. This amounts to an untwisting of crystallite ribbons close to the minor axis of the deformed spherulite, as noted above from optical microscopic studies. In the present context, this would give rise to a decrease in the absorbance of the *a*-polarised component of the CD_2 bending vibration, while the *b*-polarised component would be unaffected.

For radii parallel to the draw direction ($1_\parallel$ and $2_\parallel$ in Fig. 1), *c* is initially perpendicular to the draw direction, while *b* is along it. In this case, we could anticipate rotation of the unit cell about the local *a*-axis for all such regions. For region $1_\parallel$, both *b*- and *c*-axes stay in the sample plane during this process, while *a* remains normal to it. Both *a* and *b* polarised vibrational components would be unaffected by deformation. In region $2_\parallel$,

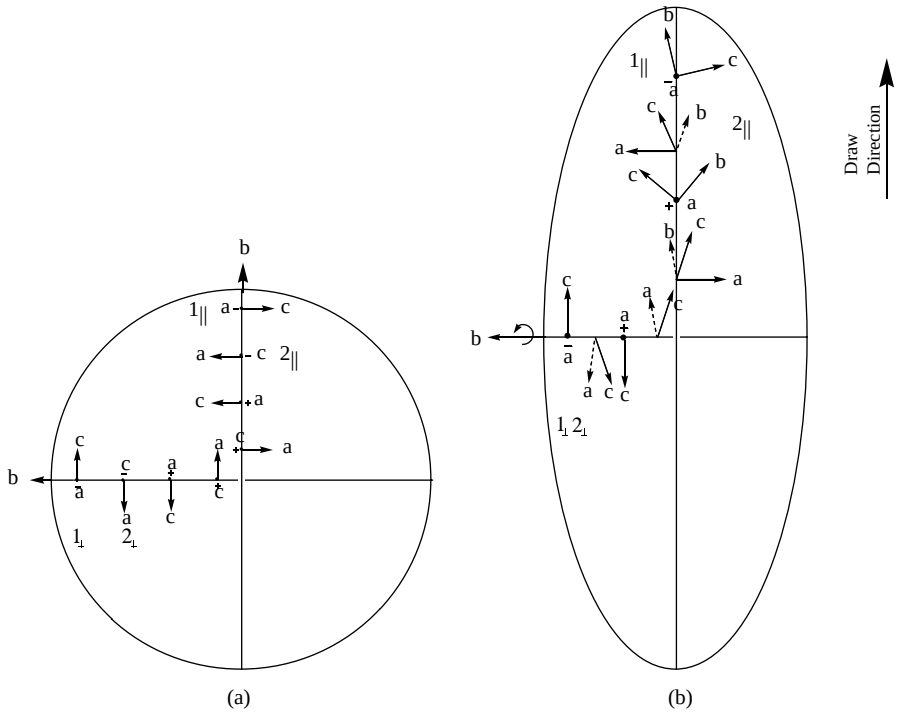

Fig. 1. Illustration (after Ref. [28]) of (a) a homogeneous spherulite, showing the periodicity in the orientation of the unit cell and (b) a deformed spherulite, showing the reorientation process. The dashed arrows represent axes leaving the sample plane and the solid arrows show axes either in or moving into the sample plane. + and −, indicate vectors pointing out of and into the plane of the sample.

rotation about *a* would now involve the movement of *b* away from the sample plane. A decrease in absorbance of the *b*-polarised component would be accompanied by no change in the *a*-polarised component. It should be noted that this mode of reorientation would disrupt the continuity of crystallite ribbons in this direction.

Finally, for radii perpendicular to both the sample plane and the draw direction, the *a*- and *c*-axes are always in the sample plane. Rotation about the *b*-axis would achieve the required *c*-axis alignment with the draw direction. The absorbance of both *a*- and *b*-polarised components would remain constant here.

The mechanisms proposed here are consistent with the observations of Hay and Keller [15]. They found evidence for rotation of the unit cell about the *b*-axis initially (up to a draw ratio of 7), while indications of rotation about the *a*-axis were only found at draw ratios of 10 and above. They concluded that radii parallel to the draw direction were initially more resistant to deformation and that rotation about the *b*-axis is easier than about the *a*-axis. More recent WAXS studies on PE stretched to a draw ratio of around 5 reinforce this conclusion [19].

The predicted effects of crystallite rotation on the CD_2 bending vibration are summarised in Table 1. We can thus anticipate the effects on the different components of the CD_2 bending vibration arising from rotation alone. Combining the predictions from Table 1, stretching should induce a decrease in absorbance of the *a*-polarised component with increasing draw ratio, while the *b*-polarised component should initially stay constant and then decrease at higher draw ratios. This latter prediction is on the basis that rotation is easier about the *b*-axis than about the *a*-axis.

The effects of intralamellar slip can also be considered here. Fig. 2 gives a schematic representation of fine and coarse slip. The former is likely to have little effect on the FTIR spectrum: provided that local arrangements of isotopically labelled crystal stems are undisturbed and chain lengths remaining 'in register' are sufficient, then the doublet splittings will be unchanged. However, any resulting change in unit cell dimensions in the *a*–*b* plane will affect the magnitude of CD_2 bending splittings. On the other hand, coarse slip will have a substantial effect on the splittings. The separation of segments of the original lamellae will break groups of labelled stems into smaller groups, with a reduction in the associated splitting. The

Table 1
Summary of the expected effects of uniaxial deformation of a spherulite, in three orthogonal directions

Spherulite radius	Axis of unit cell rotation	Effect on IR CD_2 bending mode absorbance
Parallel to draw direction	*a*	*a*–; *b*↓
Perpendicular to draw direction and in sample plane	*b*	*a*↓; *b*–
Perpendicular to draw direction and perpendicular to sample plane	*b*	*a*–; *b*–

–, indicates the absorbance of the IR component with this polarisation is unchanged; ↓, indicates the absorbance of this component decreases.

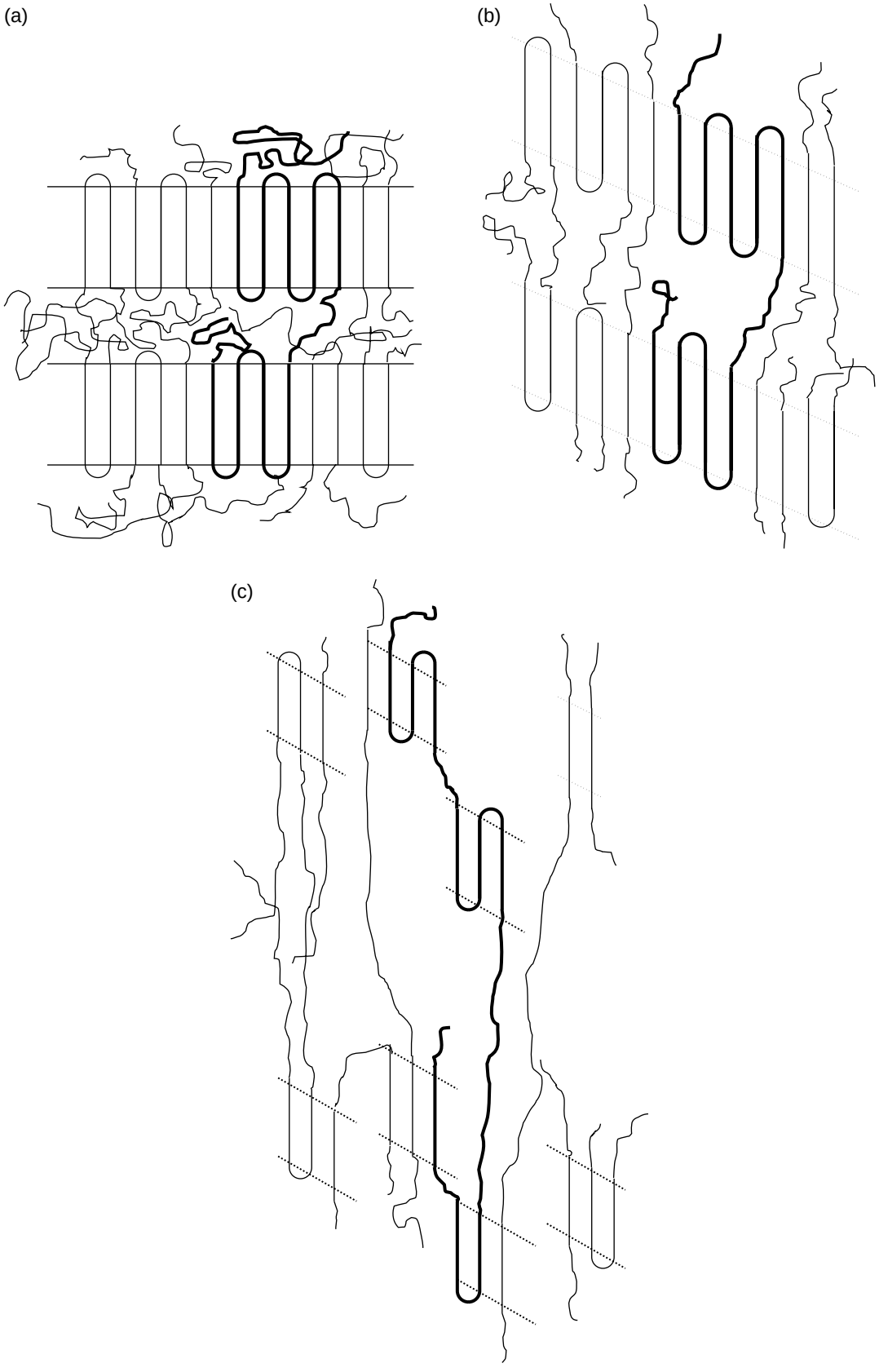

Fig. 2. (a) Initial chain-folded lamellar structure. The bold line indicates a deuterium-labelled molecule within a hydrogenous polyethylene matrix; (b) the development of chain tilt within lamellae, corresponding to fine slip. MCIRS CD_2 bending splittings are largely unaffected and (c) the process of coarse slip results in a substantial disruption of both the lamellae and the groups of labelled stems. CD_2 bending splittings are consequently reduced.

smaller the remaining crystallite segments in Fig. 2(c), the smaller would be the splittings obtained. Ultimately, at sufficiently high draw ratios, only labelled stems isolated from similar nearest neighbours would be expected to survive, producing only a singlet contribution to the spectrum. The labelled molecule in Fig. 2(c) also shows evidence of a fold being 'pulled through' the crystallite, another process which can reduce group size. The MCIRS technique, therefore, provides an important indicator of coarse slip in these systems.

Finally, we consider here the behaviour of amorphous chains. Labelled amorphous chains contribute to the singlet component of the CD_2 bending vibration. Besides any effects due to chain alignment on deformation, stress-induced crystallisation would increase the absorbance ratio of doublet to singlet contributions in the spectrum.

3. Experimental

3.1. Materials

The characterisation of the linear PE samples is given in Table 2. Linear deuterated sample 2 was kindly supplied by Dr Barham (University of Bristol). This was prepared from a commercial polymer by liquid–liquid fractionation. Linear deuterated sample 4, deuterated copolymer sample 5 and hydrogenous samples D and E were produced by BP Chemicals and kindly provided by Dr W. Reed. GPC characterisation was obtained from the groups at the University of Bristol and BP Chemicals and ^{13}C NMR from BP Chemicals.

Isotopic blending was carried out in xylene solution, using 3 or 5% w/w fully deuterated polymer previously mixed with hydrogenous PE. After precipitation from methanol, the filtered and dried samples were packaged in aluminium and heated to 160 °C in a press for 15 min before quenching into cold water. Films of approximately 0.3 mm thickness were produced in this way. Further details of sample characterisation and preparation are given in Ref. [8].

The sample nomenclature introduced in Ref. [8] is also used here. For example, LL/95/385 denotes a blend of linear deuterated PE with molecular weight 95,000 (sample 2, Table 2) and a linear host PE with molecular weight 385,000 (sample D, Table 2). CL/95/385 is a similar sample, but includes copolymer sample 5 as the guest species.

Table 2
Characterisation of guest and host polyethylene and ethylene copolymer materials used

Material identifier[a]	Type[b]	$\bar{M}_w \times 10^{-3}$	$\bar{M}_n \times 10^{-3}$	$\bar{M}_w/\bar{M}_n$	Short chain branches[c]
2	LD	95	48	2.0	–
4	LDM	413	157	2.6	–
5	CDM	95	11	8.6	6.3 C_6
D	LH	385	48	8.0	–
E	CH	181	14.9	12.1	6 C_4

[a] Nomenclature as used in Ref. [5].
[b] L, denotes a linear polymer; C, an ethylene copolymer; D, a deuterated polymer; H, a hydrogenous polymer and M, a metallocene-catalysed polymer.
[c] Short chain branch content per 1000 backbone carbon atoms, as determined by BP Chemicals, using FTIR spectroscopy.

3.2. Tensile deformation and FTIR

A Mattson Galaxy 6021 FTIR spectrometer was used, with an MCT detector. A Rheometrics Minimat tensile tester was used to draw dumbbell-shaped samples of size 1 cm × 2 cm at a rate of 1 mm min^{-1}. The local draw ratio in the region sampled by the beam was determined using an array of small ink spots, in conjunction with a travelling microscope. Measurements were made in the necked region of the sample. As space did not permit mounting the Minimat tester inside the FTIR sample compartment, a form of clamp was devised to grip a sample which had previously been stretched in the Minimat. The clamp with sample could then be installed in a Graseby-Specac 21500 cryostat, used with a 20120 temperature controller. Cooling with liquid nitrogen to temperatures of −173 °C maximised the CD_2 bending splittings observed. The sample space was evacuated and a dry air purge was employed to minimise interference from water and carbon dioxide vapour. A spectral resolution of 1 cm^{-1} was used, with typically around 100 scans. Curve fitting and Fourier self-deconvolution of spectra were carried out using Mattson software.

3.3. SAXS measurements

A Rigaku–Denki camera was used with Cu K_α radiation and a sample to film distance of 264 mm to obtain long spacings for a selection of samples (courtesy of Prof Ungar, University of Sheffield).

3.4. SANS measurements

Measurements were made using the instruments LOQ (ISIS, Didcot, England) and D11 (ILL, Grenoble, France). Further experimental details are given elsewhere [8].

4. Results

4.1. LL/95/385

Fig. 3 shows the evolution of the CD_2 bending region of the FTIR spectrum with draw ratio, with data recorded at −173 °C. Typical parameters used for the deconvolution of raw data were 1.5 cm^{-1} for the full width at half maximum absorbance of the intrinsic lineshape and 2.0 for the resolution enhancement factor. The initial impression is that the spectra of the undeformed polymer and the sample after stretching to a draw ratio of 6.7 are remarkably similar. Nevertheless, significant changes occur during the course of deformation.

The high frequency component of the CD_2 bending doublet is polarised in the *a*-direction and the low frequency component in the *b*-direction. By fitting the data to several components—the central singlet and various doublet peaks—the evolution of the normalised areas of the *a*- and *b*-polarised

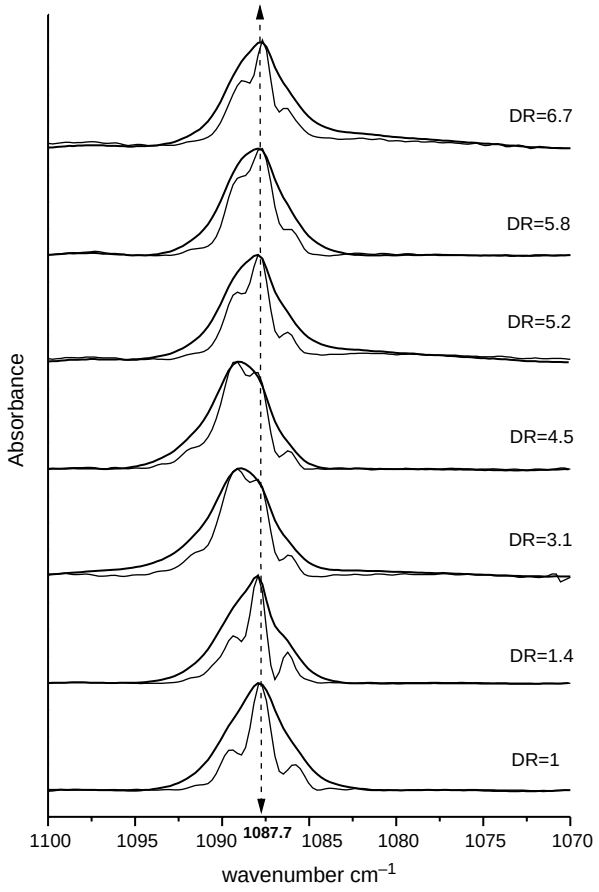

Fig. 3. Evolution of the infra-red CD_2 bending region for sample LL/95/385 with increasing draw ratio. The different draw ratios are indicated. The bold line represents raw data and the fine line deconvoluted data. The position of the singlet component at 1087.7 cm^{-1} is indicated by the vertical dashed line.

components can then be compared. Individual doublet components are often not resolved by deconvolution, due to their small separation in frequency [7]. In addition, the positions of low frequency components show a smaller dependence on splitting than the positions of high frequency ones [8]. Established relationships between the frequencies of doublet components and the corresponding splittings [8] were used to assign peaks in the deconvoluted spectra to splittings. These peak positions were then utilised for curve fitting the deconvoluted spectra. Because of the smaller separation of low frequency components, the total number of peaks was not constrained to be odd. Each peak was taken as a combination of Lorentzian and Gaussian lineshapes. The results of this curve fitting are shown in Fig. 4.

At least two stages can be identified in Figs. 3 and 4: (a) the area of the *a*-polarised components increases to a maximum around $\lambda = 4.5$, while the *b*-polarised components reach a minimum at the same draw ratio and (b) for $\lambda > 5$, the *a*-polarised components decrease in area while the *b*-polarised ones increase to a plateau around the maximum draw ratio studied. The first step can be interpreted as a progressive alignment with *a* in the plane of the sample and *b* leaving the plane. The second stage is, as will be discussed later, consistent with the development of *c*-axis orientation.

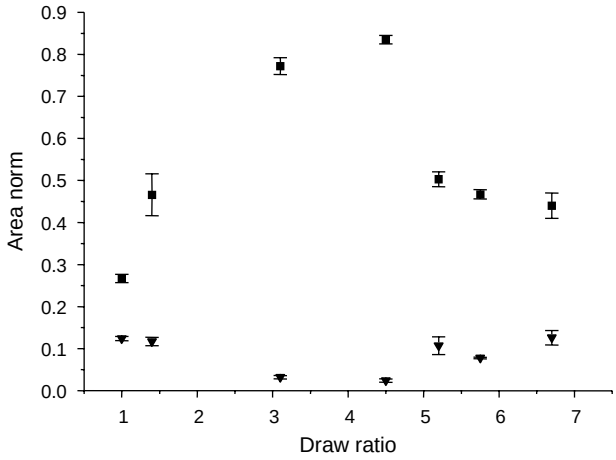

Fig. 4. Normalised areas of *a*-polarised (solid squares) and *b*-polarised (solid triangles) band components as a function of draw ratio for sample LL/95/385.

This analysis is necessarily restricted to the crystals themselves, without regard to the amorphous regions. However, it is reasonable to suppose that these are involved in chain reorganisation, particularly in the initial stages of deformation. Amorphous chains contribute to the central singlet, along with labelled crystal stems which have no isotopically similar nearest neighbour stems. It is, therefore, of interest to compare the evolution of areas of the singlet component with the sum of all doublet components, as determined by curve fitting. The results are shown in Fig. 5.

Two stages of deformation are again evident. The area of the singlet component reaches a minimum around $\lambda = 4$, with the doublet area simultaneously passing through a maximum. The second stage shows a rapid increase in the singlet absorbance. This suggests a progressive break-up of groups of adjacent stems, with absorbance being transferred from doublet components to the singlet. Conversely, the first stage suggests the conversion of singlet absorbance to doublet components, as

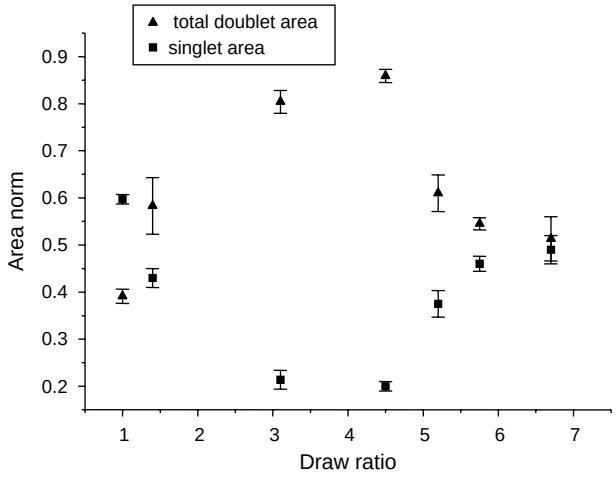

Fig. 5. Evolution of the area of the singlet and the total doublet area of the CD_2 bending peak for the sample LL/95/385, after normalisation with the total band area.

would be expected for crystallisation. Such stress-induced behaviour should result in an increase in the size of groups of adjacent labelled stems, leading to an increase in the outermost CD_2 bending splitting. This will now be investigated.

As in previous work [8] two methods were used to analyse the components of the CD_2 bending vibration. The first involved curve fitting to a singlet and the minimum number of doublet components necessary to achieve a good fit. Figs. 4 and 5 made use of this method. Normally, up to five Voigt functions were used. As noted earlier [8], the peak frequencies should not be interpreted as corresponding to the only groups present: lower frequency doublet components in particular may have very small separations. The results should be viewed as indicating 'average' group sizes present.

The second method involves the use of calculated splittings for small groups. After listing these splittings, a 'trial and error' method was used to combine the peaks to provide as close a match as possible to experimental data. While not strictly a curve fitting technique, this method has the advantage of utilising known doublet separations. Typically, this method involved the combination of around 34 Lorentzian bands.

The curve fitting method yielded the results shown in Fig. 6. The doublet splittings fall within three bands on this graph, and there is a tendency for the splitting to decrease with increasing draw ratio in each case. At $\lambda = 3.1$, a new doublet was resolved with a splitting of 7.6 cm^{-1}. Using tabulated values of doublet splitting as a function of group size [7], this corresponds to a group of 3×3 adjacent stems in ⟨110⟩ directions (i.e. three adjacent stems on each of three adjacent (110) planes). The absorbance is very low, meaning that only a very small number of stems contribute to the bands. Two possible reasons can be advanced for the creation of these new groups. Two smaller groups may become adjacent during the deformation process to form one larger group. Considering the dilution of deuterated chains in the blends used here, this is unlikely. Alternatively, deformation of the amorphous regions may result in stress-induced crystallisation. The newly formed crystals would then show a degree of adjacency depending on the prevailing conditions, including stress. This latter mechanism for the emergence of new groups is considered far more likely here. DSC measurements on samples LL/95/385/1.0 and LL/95/385/3.5 showed an increase in crystallinity from 53 to 61%, consistent with crystallisation on deformation. A decrease in the inner splitting is also found in Fig. 6, from 3.7 to 3.1 cm^{-1}. This reduction corresponds to a change in group size from 4 to three adjacent stems in ⟨110⟩ directions, This is likely to be a result of coarse slip.

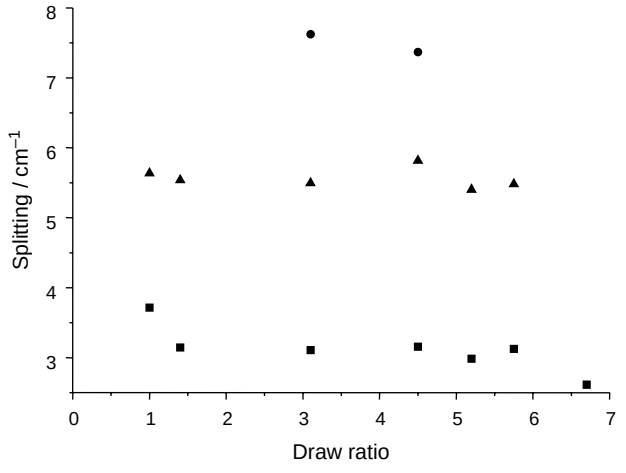

Fig. 6. Doublet splittings for sample LL/95/385 as a function of draw ratio. Filled squares indicate bands at approximately 1089 and 1086 cm^{-1}; filled triangles bands at approximately 1091 and 1086 cm^{-1} and filled circles bands at approximately 1093 and 1086 cm^{-1}.

By the time λ reached 5.2, the outermost splitting has disappeared (Fig. 6). A further doublet also vanishes on reaching the maximum draw ratio of 6.7. In addition, the innermost splitting was substantially reduced at $\lambda = 6.7$. These observations all demonstrate the progressive destruction of groups, starting at a draw ratio of around 5.

Using the alternative method of data analysis, namely synthesizing a combination of the bands arising from the known splittings of small groups, resulted in the data shown in Fig. 7. Examples of deconvoluted experimental data are shown here alongside synthesized spectra. This technique has been described in fuller detail elsewhere [8]. Allowance was made for orientational effects in the CD_2 bending region, by introducing a coefficient α to scale the low wavenumber side of the band. The proportion of stems arising from each group, N, was determined from the proportion of stems, $N_{\text{splitting}}$, used for the calculation of the profile through

$$N = \frac{\alpha_j}{\alpha_1} N_{\text{splitting}}$$

where α_j and α_1 are the scaling coefficients used to fit the low frequency profile at draw ratio j and for the undeformed sample, respectively. The match in spectra is not ideal. This can be attributed partly to the limited number of components used and partly to the fact that a Lorentzian line shape has been used for deconvolution: peaks remaining in the deconvoluted spectra are, therefore, not expected to be true Lorentzian functions. Nevertheless, the main features of the deconvoluted data are clearly reproduced. Some discontinuities are evident at large splittings in the synthesized spectra, corresponding to the cut-offs used in the Lorentzian band components.

For the purpose of analysing group populations, the groups were arbitrarily classified as 'small' (2–4 adjacent stems in one plane), 'medium' (5–7 stems in one or 2 planes) and 'large' (8–12 stems in 2 or 3 planes). The results in Fig. 8 show that the proportion of stems which are isolated falls from 65 to 50% for λ of around 3. This fall is associated with a substantial increase in the number of small groups (from 32 to 40%) and significant increases in the numbers of medium (3–6%) and large groups (0–4%). We can conclude that around 15% of initially isolated stems become incorporated in groups for a draw ratio of 3, in accordance with DSC data for crystallinity quoted earlier. For $\lambda > 4$, Fig. 8 shows that the proportion of isolated stems increases at the expense of medium and large groups. The proportion in small groups stays roughly constant. The interpretation is of small, medium and large groups

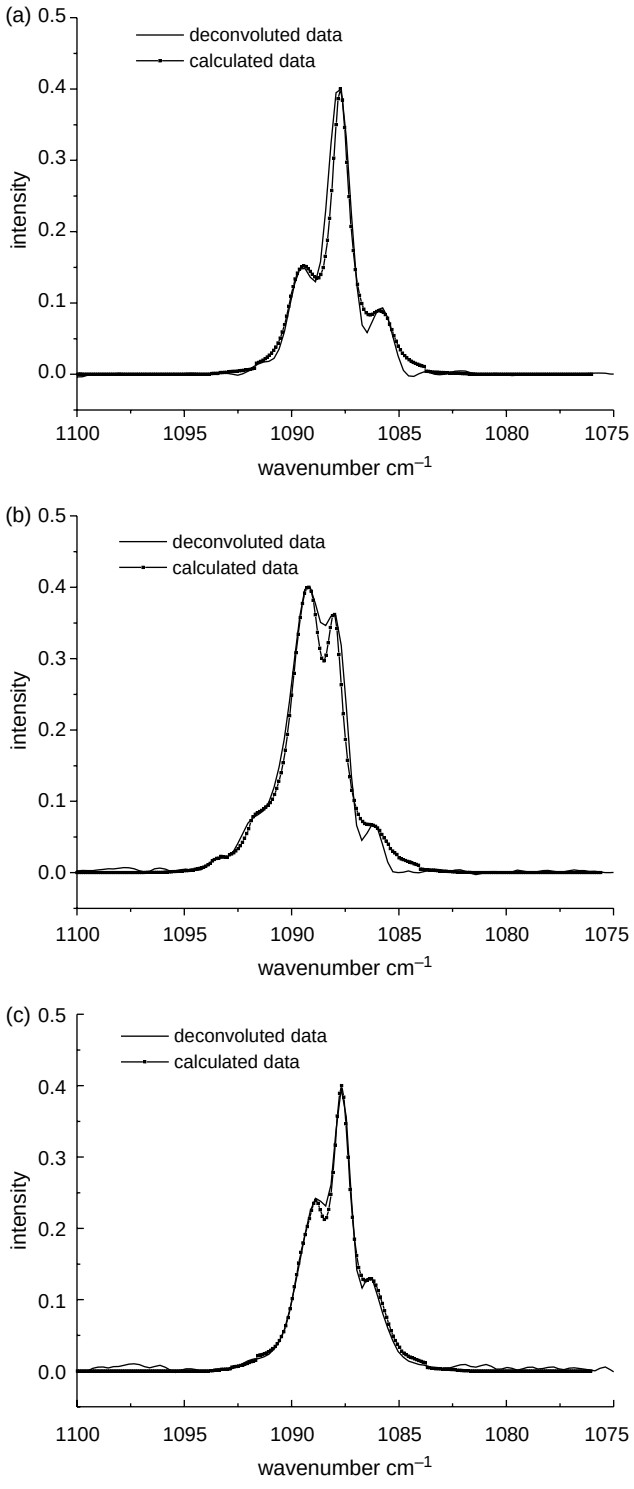

Fig. 7. An example of the 'fitting' of CD_2 bending profiles by combining splittings calculated for small groups of labelled stems and comparing with deconvoluted experimental data for sample LL/95/385 (a) shows the undeformed sample; (b) data for a draw ratio of 4.5 and (c) data for a draw ratio of 6.7. Lorentzian functions were used for all calculations.

progressively breaking up, creating more isolated stems. The proportion of small groups is maintained by their creation from break-up of larger groups balancing their destruction to form isolated stems.

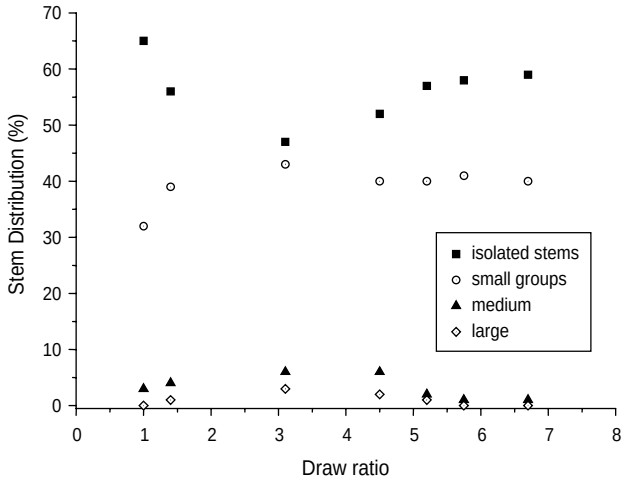

Fig. 8. Evolution of the stem distributions with draw ratio for sample LL/95/385. 'Isolated stems' correspond to the singlet; the 'small' groups include 2–4 stems in one plane (2×1, 3×1 and 4×1 groups, with splittings between 2.6 and 3.9 cm^{-1}) and contribute to the inner doublets; the 'medium' groups include 5–7 stems in 1 or 2 planes (5×1, 2×2 and 3×2 groups, with splittings of 4.2–6.1 cm^{-1}) and contribute to the intermediate doublets and the 'large' groups include 8–12 stems in 2 or 3 planes (4×2, 5×2, 3×3 and 4×3 groups, with splittings of 6.4–8.1 cm^{-1}) and contribute to the outermost doublet.

It is worth noting that the CH_2 wagging region of the low temperature FTIR spectrum, which is sensitive to chain conformations involving gauche bonds, shows a continuous increase in absorbance for all related bands with increasing draw ratio. This suggests that crystal defects are an important feature at all levels of deformation. This is in accordance with Raman spectroscopic studies of uniaxially stretched HDPE and several branched materials, which indicated a reduction in crystallinity as compared with data from other techniques [20]. This was interpreted as indicating a highly disrupted orthorhombic crystalline morphology, a view consistent with our interpretation.

Evidence of the Martensitic transformation to the monoclinic phase was provided by the appearance of a 716 cm^{-1} peak in the CH_2 rocking region for drawn samples.

4.2. LL/413/385

In this section, a similar approach is adopted to the data analysis as in the previous one. Fig. 9 shows the CD_2 bending region of the FTIR spectrum as a function of draw ratio. Similar deconvolution parameters were used. Spectra show significant changes with draw ratio: there is a clear reduction in the number of peaks apparent after deconvolution, with increasing draw ratio.

As with sample LL/95/385, the *a*-polarised component initially increases in absorbance with draw ratio. However, the second stage observed for LL/95/385, involving a decrease in this absorbance, was not observed here, even at the highest draw ratio.

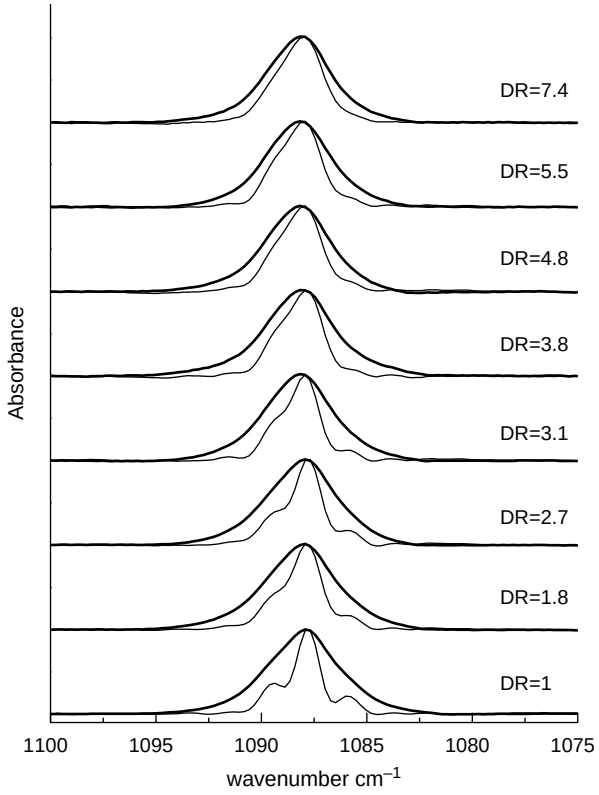

Fig. 9. Evolution of the infra-red CD_2 bending region for sample LL/413/385 with increasing draw ratio. The different draw ratios are indicated. The bold line represents raw data and the narrow line deconvoluted data.

As previously, the initial analysis involved fitting the band profiles to a central singlet and doublet components. This enables a separation of *a*-polarised (higher frequency) and *b*-polarised (lower frequency) components. The results are shown in Fig. 10. As noted above, the *a*-polarised component increases in absorbance with draw ratio, although this change is seen from Fig. 10 to be slight. The *b*-polarised bands show a more significant decrease in absorbance. There is some

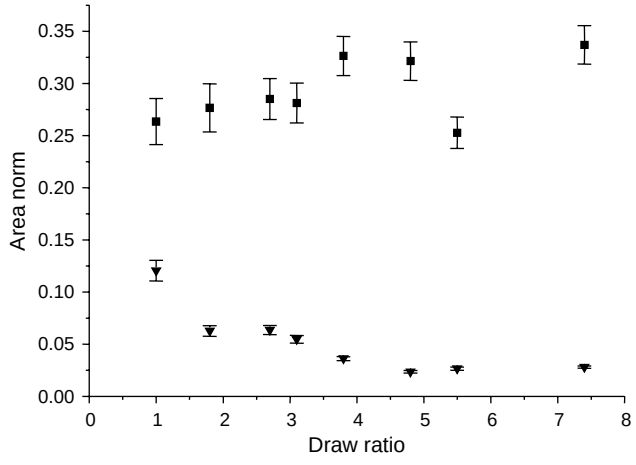

Fig. 10. Normalised areas of *a*-polarised (solid squares) and *b*-polarised (solid triangles) band components as a function of draw ratio for sample LL/413/385.

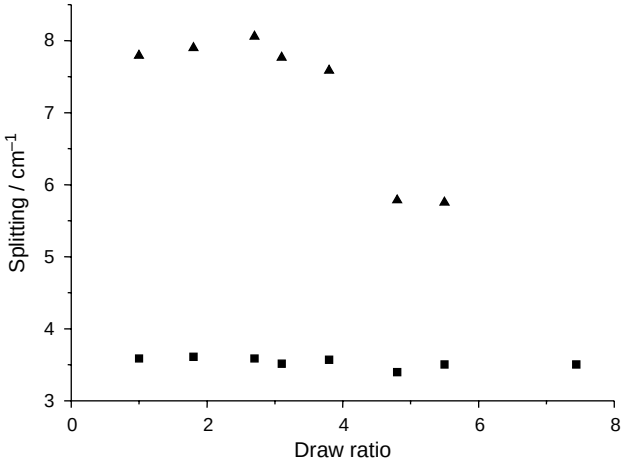

Fig. 11. Doublet splittings for sample LL/413/385 as a function of draw ratio. Filled squares indicate bands at approximately 1089 and 1086 cm^{-1}; filled triangles bands at approximately 1091 and 1083 cm^{-1} at low draw ratios (<4.5) and approximately 1091 and 1086 cm^{-1} at draw ratios above 4.5.

indication that, for both polarisations, a plateau is reached for draw ratios above about 4.

The area of the singlet peak shows a slight increase with increasing draw ratio, with the total doublet area showing a slight decrease. As in the previous sample, this can be interpreted as the result of the break-up of groups of adjacent stems, although here the effect is small. The doublet splittings obtained from curve fitting are shown in Fig. 11. In most cases, two doublets were resolved, the inner splitting having a constant value of around 3.5 cm^{-1}, corresponding to groups of 3×1 or 4×1 adjacent labelled stems. For draw ratios up to around 3, there is a slight increase in the outermost splitting to a value of 8.1 cm^{-1}. This appears to indicate a small proportion of stress-induced crystallisation. At higher draw ratios, the splitting decreases significantly to 5.8 cm^{-1} (a change from 3×3 groups to 3×2), before disappearing at draw ratios above 5.5. This provides further evidence for the destruction of groups of stems.

The alternative technique of synthesizing band combinations, using known small group splittings, was again used. It was found necessary to increase the width of the singlet component used in this 'fitting' process with increasing draw ratio and the change is shown in Fig. 12. A Voigt shape function was used for this singlet and it was found that the Lorentzian component needed to be reduced and the Gaussian one increased with increasing draw ratio. Furthermore, a frequency shift of $+0.24$ cm^{-1} was noted in the peak position, when comparing the undrawn sample with one with a draw ratio of 1.8. These observations suggest a change in shape of the singlet component on deformation. One possible cause could be the formation of the monoclinic crystal form. However, the continuous nature of the change shown in Fig. 12 seems to contradict the evidence that the proportion of monoclinic form reaches a plateau level with increasing deformation [9,21]. Alternatively, the bandwidth may reflect the range of environments of isolated labelled stems, for

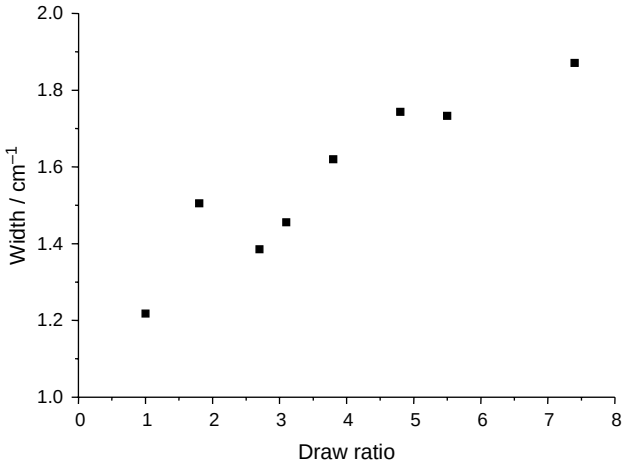

Fig. 12. Change in width of the singlet component for sample LL/413/385 with draw ratio, obtained from the curve fitting analysis, using a Voigt shape function for fitting the singlet.

example in terms of strain. Such an effect might arise from the presence of tie molecules.

The development of group size with drawing is shown in Fig. 13 for this method of analysis. The (arbitrary) classification of small, medium and large groups is slightly different from that used in Fig. 8, since the maximum group size is larger. The number of isolated stems increases from 68% before drawing to 79% at a draw ratio of 7.4. As noted earlier, sample crystallinity increases with drawing, which would result in a decrease in the proportion of isolated stems. The observed increase is, therefore, related to isotopically isolated stems within crystals. The proportion of medium and large groups generally decreases with increasing draw ratio, ultimately reaching zero. Small groups show an initial decrease in number, reaching a constant value for a draw ratio of about 4. The increase in the proportion of isolated stems at the expense of groups is similar to the behaviour of sample LL/95/385 at higher draw ratios. It can similarly be attributed to a progressive crystal break-up. However, in this case it occurs over the whole deformation range studied. In the present case, evidence for stress-induced crystallisation is more subtle: there is a small increase in the proportion of 'medium' groups on stretching to a draw ratio of 1.8 (Fig. 13) and the evolution of *a*- and *b*-polarised bands with deformation is consistent with oriented crystallisation of amorphous material. However, this phenomenon is not apparent from group size distributions.

The CH_2 wagging region for this sample also showed an initial increase in all band absorbances with draw ratio, but a plateau level appeared to be reached by a draw ratio of around 4.

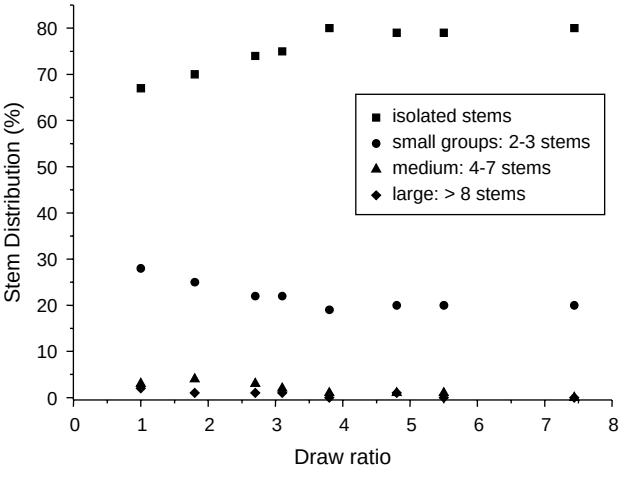

Fig. 13. Evolution of the stem distributions with draw ratio for sample LL/413/385. 'Isolated stems' correspond to the singlet; the 'small' groups include 2–4 stems in one plane (2×1, 3×1 and 4×1 groups, with splittings between 2.6 and 3.9 cm^{-1}) and contribute to the inner doublets; the 'medium' groups include 5–7 stems in 1 or 2 planes (5×1, 2×2 and 3×2 groups, with splittings of 4.2–6.1 cm^{-1}) and contribute to the intermediate doublets and the 'large' groups include 8 or more stems in 2 or 3 planes (4×2 and larger groups, with splittings of 6.4 cm^{-1} and above) and contribute to the outermost doublet.

4.3. CL/95/385

The guest molecular weight of this sample was chosen to match that of a linear guest material used in Section 4.1, enabling a direct comparison with sample LL/95/385. The evolution of the CD_2 bending region of the FTIR spectrum with draw ratio is shown in Fig. 14. Spectra were recorded at −173 °C. Typical deconvolution parameters used were again 1.5 cm^{-1} for the FWHM absorbance of the intrinsic lineshape and 2.0 for the resolution enhancement factor. Little change in

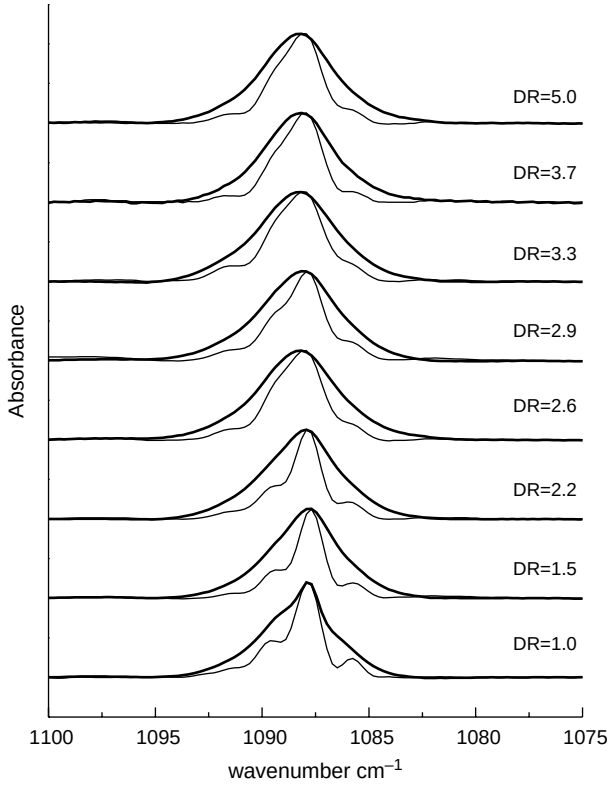

Fig. 14. Evolution of the infra-red CD_2 bending profile for sample CL/95/385 with increasing draw ratio. The different draw ratios are indicated. The bold line represents raw data and the fine line deconvoluted data.

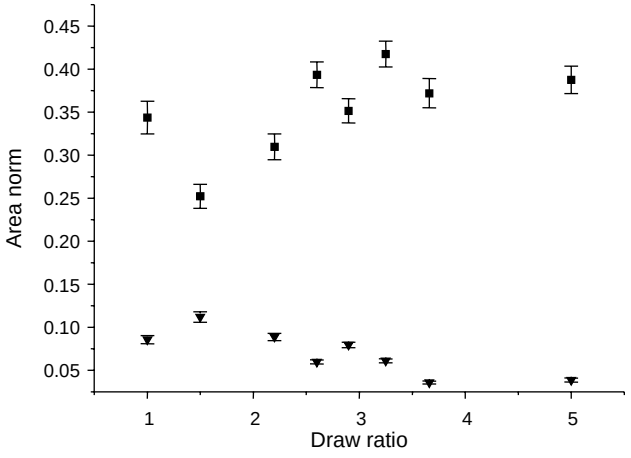

Fig. 15. Normalised areas of *a*-polarised (solid squares) and *b*-polarised (solid triangles) band components as a function of draw ratio for sample CL/95/385.

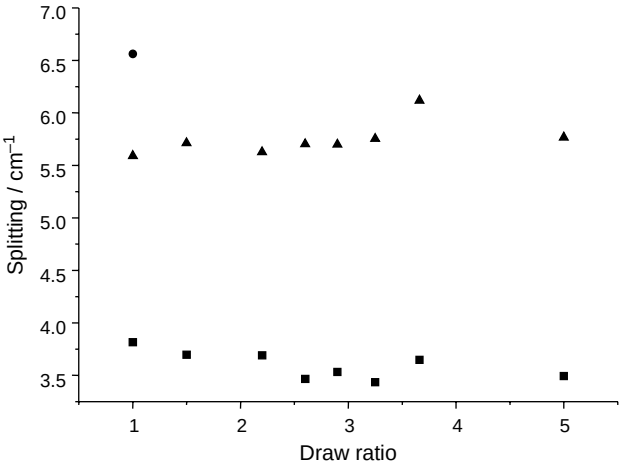

Fig. 16. Doublet splittings for sample CL/95/385 as a function of draw ratio. Filled squares indicate bands at approximately 1089 and 1086 cm^{-1}; filled triangles bands at approximately 1091 and 1086 cm^{-1} and filled circles bands at approximately 1092 and 1086 cm^{-1}

the profile is immediately apparent for draw ratios below 2.6. Spectra at higher draw ratios show higher absorbance to the high frequency (*a*-polarised) side of the band. Contrary to data for LL/95/385, there is a significant change in the form of the spectrum with drawing. A simple curve fitting to deconvoluted data allows a separation of singlet, *a*-polarised and *b*-polarised components of the spectrum, since the high and low frequency doublet components are polarised in the *a*- and *b*-directions, respectively. This is shown in Fig. 15. The early stages of deformation, up to a draw ratio of 1.5, shows an enhancement of the *b*-polarised component and a corresponding increase in the *a*-component. The remainder of the range of deformation shows a gradual increase in the *a*-polarised component and a decrease in the b-component, similar to that observed for linear polyethylene (PE) sample LL/413/385. As in that case, the changes in area are relatively small and both areas appear to have reached plateau values by a draw ratio of around 4. The interpretation is similar: the crystallographic *a*-axis moves into the sample plane and the *b*-axis moves out of the plane as a result of the crystallisation of amorphous material. The observation of plateau values can be understood in terms of lamellae within spherulites. We again suggest that an untwisting occurs in spherulite ribbons along radii perpendicular to the draw direction and in the sample plane. On its own, this would lead to a decrease in the *a*-polarised area. Here it is believed to compensate for the ordering of amorphous chains at the higher draw ratios.

As previously [8], two methods were used for data analysis. The first involved curve fitting to a central singlet and various doublets, while the second was a trial-and-error method using splittings calculated for small groups of labelled crystal stems to match experimental data.

The first of these methods yielded the doublet splittings shown in Fig. 16. The undrawn sample shows three doublets. The outermost splitting of 6.5 cm^{-1} (corresponding to around 4×2 groups of adjacent labelled stems in ⟨110⟩ directions, using tabulated calculations of doublet splittings as a function of group size [7]) disappears on deformation. However, it should be noted that the small initial absorbance indicates a very small proportion of stems involved. The other two doublets show little variation in splitting on deformation. One has a splitting of around 3.7 cm^{-1}, corresponding to groups of 3×1 or 4×1 stems, while the other lies between 5.6 and 6.1 cm^{-1}, corresponding to groups of around 3×2 stems.

The simulation of CD_2 bending spectra, using the splittings calculated for specific small groups of labelled stems, showed that the width of the central singlet increased with drawing. Similar behaviour was noted above for sample LL/413/385, and we suggest the same reason, namely strained bonds. However, the guest molecular weight makes it unreasonable to suppose that these are due to tie molecules. After categorising groups of labelled stems as small (2–3 stems), medium (4–7 stems) and large (8–12 stems), the evolution of these groups with deformation is shown in Fig. 17. The results differ significantly from those observed for blends of linear polymers (Sections 4.1 and 4.2 above). At low levels of deformation (draw ratio, $\lambda \leq 1.5$), the proportions of isolated stems and small groups increase slightly at the expense of medium and large groups. This is consistent with the disappearance of the outermost splitting in Fig. 16. The behaviour up to a draw ratio of around 3.5 is consistent with stress-induced crystallisation: the number of isolated stems decreases, while the number of stems in groups of any size increases. At draw ratios beyond 3.5, there is a change in behaviour. The number of isolated stems increases to beyond the value for the undrawn sample, while the number in groups of all sizes decreases. This demonstrates the process of coarse slip, causing blocks within crystallites to become detached from one another, as shown in Fig. 2. Comparing Figs. 15 and 17, it appears likely that the processes of reorientation of crystalline lamellae and crystallite break-up show some overlap in the deformation ranges concerned. Nevertheless, the overall behaviour is generally more similar to that of sample LL/95/385 than to that of LL/

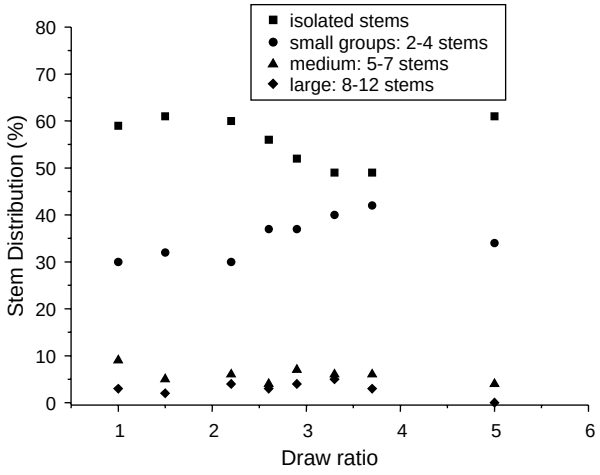

Fig. 17. Evolution of the stem distributions with draw ratio for sample CL/95/385. 'Isolated stems' correspond to the singlet; the 'small' groups include 2–4 stems in one plane (2×1, 3×1 and 4×1 groups, corresponding to splittings between 2.6 and 3.9 cm^{-1}) and contribute to the inner doublets; the 'medium' groups include 5–7 stems in 1 or 2 planes (5×1, 2×2 and 3×2 groups, with splittings of 4.2–6.1 cm^{-1}) and contribute to the intermediate doublets and the 'large' groups include 8–12 stems in 2 or 3 planes (4×2, 5×2, 3×3 and 4×3 groups, with splittings of 6.4–8.1 cm^{-1}) and contribute to the outermost doublet.

413/385, with a clearer separation of the ranges of crystallisation and of coarse slip.

4.4. CC/95/181

Previous SANS and MCIRS studies have shown that the combination of copolymer guest and host species leads to a more compact molecular conformation, with a greater proportion of adjacent crystal stems [8]. The conformational evolution with deformation might thus be expected to differ.

Fig. 18 shows the development of the CD_2 bending region with deformation. Once again there are clear changes with drawing, particularly beyond a draw ratio of 2.7. Curve fitting confirms that the *a*- and *b*-polarised peak areas (Fig. 19) change little until the draw ratio exceeds 2.7. The *a*-polarised area then increases progressively up to the limit of the deformation range, while the *b*-polarised area initially decreases before passing through a minimum at a draw ratio of around 3.5–4.0. After the initial stage of deformation showing negligible change, the behaviour in Fig. 19 appears similar to that of sample CL/95/385 (Fig. 2) and sample LL/413/385. It would appear that crystallisation of amorphous material is again involved.

Curve fitting of deconvoluted data revealed the doublet splittings shown in Fig. 20. The initial splittings of 8.5, 6.9 and 3.5 cm^{-1} correspond to groups of 6×3, 5×2 and 3×1 stems, respectively. The splittings are virtually unchanged up to a draw ratio of 2.7. Beyond this level of deformation, the outermost splitting, albeit involving a very small number of stems, disappears. The intermediate splitting is reduced to 5.4 cm^{-1}, corresponding to 2×2 or 3×2 groups, at a draw ratio of 3.4 and the splitting shows a further small decrease at

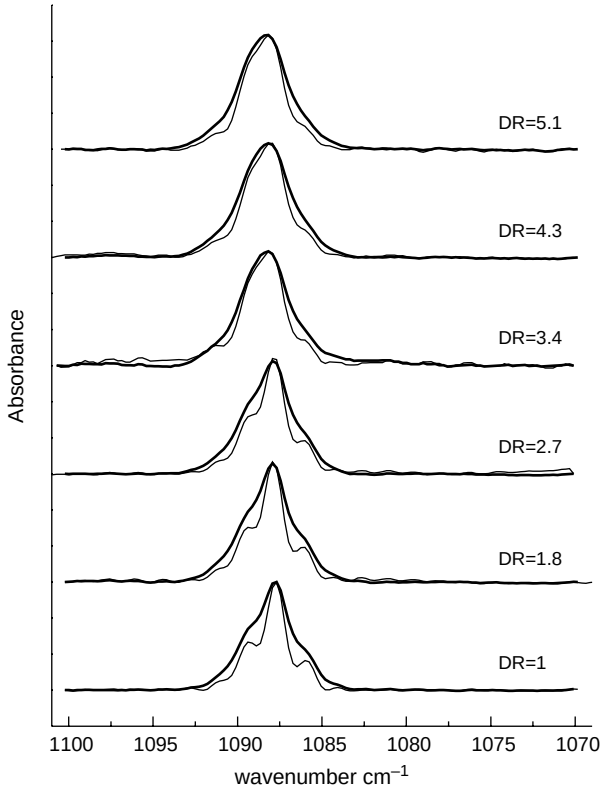

Fig. 18. Evolution of the infra-red CD_2 bending profile for sample CC/95/181 with increasing draw ratio. The different draw ratios are indicated. The bold line represents raw data and the fine line deconvoluted data.

higher draw ratios. The innermost splitting does not change significantly throughout the deformation range.

The simulation of CD_2 bending spectra again showed an increase in the width of the central singlet with the level of deformation. Fig. 21 shows the evolution of group populations with deformation, with similar categories of group size as those used in Fig. 17. Up to a draw ratio of 3.4, the number of isolated stems decreases while the numbers of stems in small and medium groups increases. The number of stems in large groups

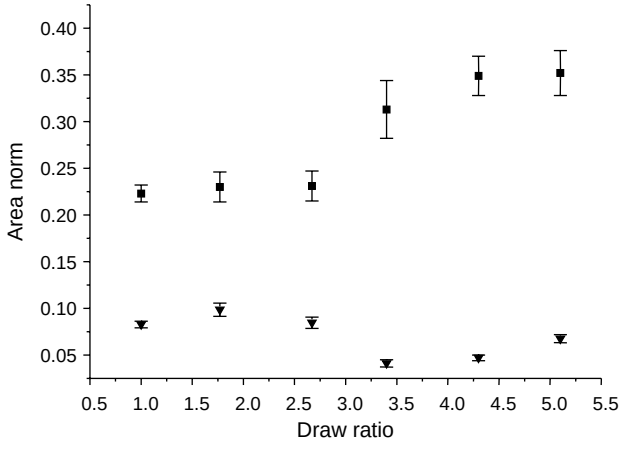

Fig. 19. Normalised areas of *a*-polarised (solid squares) and *b*-polarised (solid triangles) band components as a function of draw ratio for sample CC/95/181.

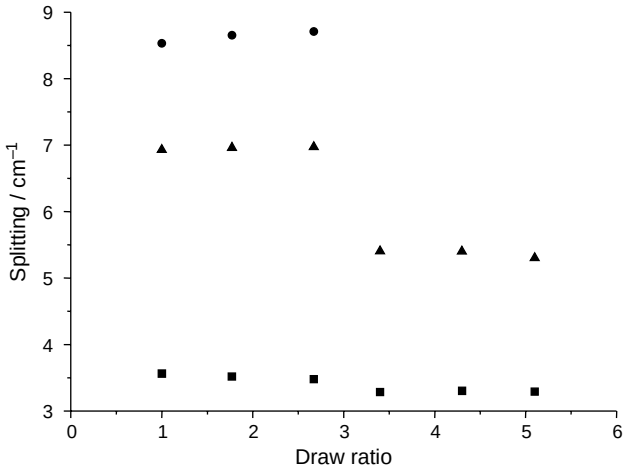

Fig. 20. Doublet splittings for sample CC/95/181 as a function of draw ratio. Filled squares indicate bands at approximately 1089 and 1086 cm^{-1}; filled triangles bands at approximately 1091 and 1086 cm^{-1} and filled circles bands at approximately 1093 and 1086 cm^{-1}.

falls to zero at a draw ratio of 3.4. This is consistent with crystallisation of amorphous polymer, together with a limited amount of crystal break-up. For draw ratios greater than 3.4, the number of isolated stems increases while the number in small and medium groups decreases. This shows that crystal break-up is happening increasingly.

5. Discussion

5.1. Linear guest molecules

The behaviour of sample LL/95/385 can be divided into three stages: (i) the crystallisation of amorphous polymer; (ii) the untwisting of crystallite ribbons perpendicular to the draw direction and in the sample plane and (iii) the progressive break-up of crystallite ribbons through coarse slip.

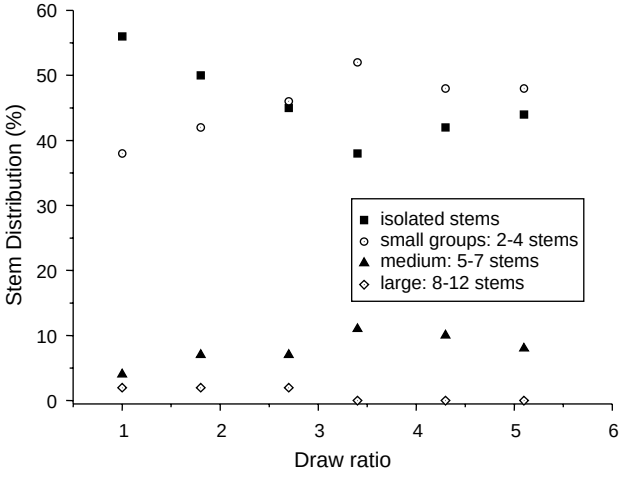

Fig. 21. Evolution of the stem distributions with draw ratio for sample CC/95/181. 'Isolated stems' correspond to the singlet; the 'small' groups include 2–4 stems in one plane (2×1, 3×1 and 4×1 groups, corresponding to splittings between 2.6 and 3.9 cm^{-1}) and contribute to the inner doublets; the 'medium' groups include 5–7 stems in 1 or 2 planes (5×1, 2×2 and 3×2 groups, with splittings of 4.2–6.1 cm^{-1}) and contribute to the intermediate doublets and the 'large' groups include 8–12 stems in 2 or 3 planes (4×2, 5×2, 3×3, 4×3 and 5×3 groups, with splittings of 6.4–8.3 cm^{-1}) and contribute to the outermost doublet.

With regard to the first stage, melting and recrystallisation have frequently been associated with polymer deformation. In this work, all drawing was carried out at room temperature. Earlier SANS measurements indicated the absence of melting and recrystallisation under these conditions [22]. It could be argued that the appearance here of large, new CD_2 bending doublets with drawing (Fig. 6) is consistent with melting and recrystallisation, but SANS data indicate an absence of isotopic fractionation [5]. We conclude that crystallisation of amorphous chains is the major process, particularly in view of the substantial increase in crystallinity (from 53 to 61% at a draw ratio of 3.5).

Evidence for the first stage comes primarily from MCIRS data. The initial increase in absorbance of the *a*-polarised components of the CD_2 bending vibration (Fig. 4) cannot be explained by the mechanism of rotation within the crystallites shown in Fig. 2(b). It is unlikely, at such low draw ratios, that the simultaneous decrease observed in the *b*-polarised absorbance is related to a rotation of unit cells about the *a*-axis in radii parallel to the draw direction. We conclude that crystallisation occurs with the *a*-axis preferentially aligned within the sample plane and the *b*-axis out of this plane. Evidence from electron microscopy would be needed to confirm this arrangement. As an aside, it is interesting to note that this has similar features to the crystallite morphology of extruded LDPE [23]. From Fig. 5, it is clear that at the lower draw ratios the singlet area decreases, while the doublet area increases and this again is consistent with crystallisation. The splitting of 7.6 cm^{-1} in Fig. 6 is attributed to such newly formed crystals. DSC evidence was quoted above for the increase in crystallinity with deformation, and there are similar reports in the literature [24–26]. Indeed, previous work has related this crystallisation to interlamellar tie molecules [24,25].

The second stage in deformation—presumably following the yield point—is clear from both SANS and MCIRS measurements. SANS measurements [5] indicate departure from affine behaviour at relatively low levels of deformation (at a draw ratio of about 2). This is consistent with the suggestion that deformation of crystallites becomes significant around this level of deformation. From MCIRS, the decrease in absorbance of the *a*-polarised CD_2 bending components above a draw ratio of around 4 can be interpreted as evidence for the deformation of spherulites along radii perpendicular to the draw direction and in the sample plane. This would involve unit cell rotation about the *b*-axis and we note that this has previously been reported to be easier than rotation about *a* [15]. It corresponds to the untwisting of lamellar ribbons in this case. The data shown in Fig. 4 suggest that this process continues up to the highest draw ratios studied ($\lambda = 6.7$).

The break-up of crystallites through coarse slip occurs at the same time as the untwisting of ribbons in favourable directions. The rapid decrease in CD_2 bending doublet component area and corresponding increase in singlet area for draw ratios

above 4 (Fig. 5) provide evidence for this. This means that rotation of the unit cell about both *a*- and *b*-axes is implicated. Curve fitting shows that the largest doublet splitting progressively decreases with increasing draw ratio. This signifies crystal break-up, as shown in Fig. 2, with groups of labelled stems becoming smaller. The evolution of group sizes, as shown in Fig. 8, reveals a similar picture. It is noteworthy that for the range of draw ratios considered here, the proportion of 'small' groups remains fairly constant. The fact that the number of isolated stems increases while the numbers of medium-sized and large groups decrease suggests a dynamic situation. Nevertheless, changes to the CD_2 bending profile on deformation are seen to be much more limited than in the case of rolled PE single crystals [9], where a similar mechanism of coarse slip was proposed. In the latter case, the groups of labelled stems prior to deformation are significantly larger, so that a limited amount of deformation has a major effect on the sizes of surviving groups.

A comparison between the smallest doublet splitting obtained for this sample before deformation and that after reaching a draw ratio of 6.7 (Fig. 6) shows the extent of the corresponding groups has reduced from about 4 to 2 stems in a single plane. This suggests that the size of the surviving groups is reduced from around 18 to 9 Å. Whereas the latter figure relates to the size of crystallite blocks remaining, the former is clearly smaller than the lateral extent of undeformed crystallites: doublet splittings are only affected once the block size has been reduced to dimensions similar to those of labelled groups.

Preferred chain slip of (100) planes in PE has generally been attributed to [001](100) slip systems [15,19]. In their study of PE under compression, Galeski et al. correlated crystal rotation about the *b*-axis with the activation of [001](100) slip systems [27], so there is some precedent for the untwisting of lamellar ribbons accompanying coarse slip and crystal break-up.

Turning now to sample LL/413/385, the CD_2 bending vibration shows clear changes with deformation (Fig. 9). However, changes in absorbance of the *a*- and *b*-polarised components are small (Fig. 10) by comparison with sample LL/95/385. The small increase in *a*-polarised absorbance can again be attributed to stress-induced crystallisation.

Fig. 11 shows an initial decrease in the maximum doublet splitting around $\lambda = 4$ and the disappearance of larger splittings for draw ratios above 6. Although the change in doublet absorbance indicates some crystallite break-up throughout the deformation range studied, Fig. 11 shows that this process occurs mainly at draw ratios above 4. The processes of crystallisation and coarse slip are not so easily separable in terms of the range of deformation involved as for sample LL/95/385. Although there is no region where we can observe a decrease in *a*-polarised absorbance, the untwisting of lamellar ribbons arranged perpendicular to the draw direction and in the sample plane presumably accompanies the crystallisation of amorphous material. Similarly, the break-up of crystallites on radii parallel to the draw direction would be expected to reduce the *b*-polarised absorbance, an effect which is not observed here, despite clear evidence of crystallite break-up.

Table 3
A comparison between SAXS long period and SANS radius of gyration values as a function of guest molecular weight and molecular type

Sample	L_{SAXS} (Å)	R_g (Å)
LL/95/385	254 ± 13	279 ± 10[a]
LL/413/385	269 ± 7	524 ± 30[a]
CL/95/385	259 ± 14	209 ± 14[b]
CC/95/181	185 ± 15	237 ± 18[b]

[a] Weighted averages of data from LOQ (ISIS) and D11.
[b] Data from D11 instrument, ILL.

In considering the effect of guest molecular weight on deformation behaviour, it is useful to compare the radii of gyration and the SAXS long periods for the two undrawn samples. These are shown in Table 3.

Long period values show no significant difference, since the sample matrix is the same, and the radius of gyration for LL/95/385 is very close to its long period. However, for sample LL/413/385 the radius of gyration is almost double the long period. This suggests that a guest molecule here occupies more than one lamella, on average, indicating the presence of tie molecules. Some behavioural aspects may, then, be attributed to tie molecules.

The main difference in behaviour noted here is the completion of stress-induced crystallisation at an earlier stage of deformation in the case of sample LL/95/385. This may be related to a proportion of fractionation by molecular weight during crystallisation (it should be noted that isotopic fractionation has been shown to be unimportant here [8]). A different molecular weight population may thus be involved in the crystallisation.

5.2. Copolymer guest molecules

It was noted earlier [8] that samples with a copolymer guest species, as used in the present work, have a somewhat smaller radius of gyration than the 'baseline' linear blend LL/95/385 considered above, for the same guest molecular weight. In addition, the evolution of the radius of gyration with molecular weight was found to differ, with a smaller molecular weight exponent in the case of copolymer guest molecules [8].

In the deformation behaviour reported here, further differences can be seen. It has previously been noted [5] that copolymer guest samples of the type studied here follow an affine deformation to higher draw ratios than for blends of purely linear polymers. While the same basic processes occur (namely crystallisation of amorphous polymer, untwisting of crystallite ribbons and the progressive break-up of these ribbons), the onset of crystallisation is delayed here to higher draw ratios: Fig. 17 shows this effect for sample CL/95/385, with crystallisation occurring at draw ratios above 2. For sample CC/95/181 on the other hand, crystallisation has already started by a draw ratio of 2 (Fig. 21).

For draw ratios above 2, the evolution of *a*- and *b*-polarised CD_2 bending components for sample CL/95/385 is very similar to that observed for sample LL/413/385: the *a*-polarised area

increases while the *b*-polarised area decreases, both quantities reaching plateau values towards the end of the deformation range studied. However, the development of doublet splittings is different, with the largest splittings disappearing for CL/95/385 at the start of deformation (Fig. 16), without further changes. On the other hand, doublet splittings for LL/413/385 show progressive changes throughout the range of deformation. The behaviour of crystal stem distributions is also markedly different, with the behaviour for sample CL/95/385 (Fig. 17) showing more similarities with sample LL/95/385. It is noticeable that the reduction in the number of isolated stems for sample CL/95/385, together with the increase in number of stems in small groups, only starts at draw ratios above a value of 2, unlike the situation with LL/95/385, where these changes occur at the lowest draw ratios studied. These changes are indicative of crystallisation of amorphous material although, in the case of a copolymer guest, the process is delayed to higher draw ratios. This again appears to involve a preferred orientation with the *a*-axis in the sample plane and the *b*-axis perpendicular to it. This process occurs over a wide range of deformation, as for LL/95/385. Only at a draw ratio of around 5 have *a*- and *b*-polarised components reached plateau values (Fig. 15), from which the start of untwisting of spherulitic lamellae can be inferred. This process would have the effect of reducing the area of the *a*-polarised component, while the *b*-polarised component should remain constant. The plateaux are, therefore, likely to result from a combination of oriented crystallisation and lamellar untwisting. We conclude that the untwisting mechanism is also delayed, by comparison with linear blends, to higher levels of deformation.

In search of the cause of the postponement of both oriented crystallisation and lamellar untwisting in sample CL/95/385 by comparison with its linear counterparts, we may consider the respective X-ray long spacings and radii of gyration. Table 3 shows the relevant data. The similarity of L_{SAXS} and R_g values for sample CL/95/385 suggests that each copolymer chain is restricted to approximately one lamella. Tie molecules are, therefore, unlikely and we are led to conclude that differences in deformation behaviour for samples LL/95/385 and CL/95/385 result from chemical differences: it appears that the hexyl branches cause the delay in crystallisation and lamellar untwisting.

The process of coarse slip in CL/95/385 is evident in the latter part of Fig. 17, where the number of isolated stems increases and the number of stems in all groups is reduced. Indeed, the number of stems in 'large' groups is reduced to zero at the highest draw ratio of 5. The maximum doublet splitting (Fig. 16) is reduced from 6.5 cm^{-1} for the undrawn sample to 5.8 cm^{-1} at the maximum draw ratio. This corresponds to a reduction in group size from close to 4×2 to between 2×2 and 3×2.

Moving to sample CC/95/181, a small initial increase in the outermost splitting (Fig. 20) is accompanied by no significant change in the area of *a*- or *b*-polarised components (Fig. 19). This suggests that oriented crystallisation only occurs to a minor extent until the draw ratio exceeds 2.5. This delay in the onset of such crystallisation may also be attributable to the effect of branching. The distribution of groups (Fig. 21) shows evidence for crystal breakup, with an increasing proportion of isolated stems and a reduction in the numbers of stems in groups for draw ratios above 3.5. The areas of both *a*- and *b*-polarised components appear to reach plateau values for draw ratios above 4.0 (Fig. 19), indicating the untwisting of lamellae along spherulitic radii perpendicular to the draw direction. A comparison of L_{SAXS} and R_g values in Table 3 suggests that, on average, a guest molecule occupies slightly more than one lamella. Tie molecules might, therefore, have some influence here.

In summary, the use of a copolymer guest molecule gives rise to the same phenomena as were observed for linear polymers. However, it appears that both stress-induced crystallisation and untwisting of spherulitic lamellae are delayed to higher draw ratios than for linear materials. A study of the deformation behaviour of linear and branched polyethylene by synchrotron X-ray scattering also pointed to a delay in the activation of crystalline deformation mechanisms to higher degrees of deformation in the case of branched polymers [29]. Earlier studies have indicated a preferential exclusion of branches from within lamellae, for both polymers [30,31] and long chain *n*-alkanes [32]. At the low levels of branching in the materials studied here (Table 2), this should be particularly true. The necessity to avoid the presence of branches in the formation of new crystals may explain the observed delay in onset of crystallisation, while the delay in untwisting of spherulitic lamellae may be attributed to the difficulty in pulling branches through the lamellae.

6. Conclusions

The MCIRS technique, which has seldom previously been applied to deformed PE, is shown here to provide comprehensive detail of changes in molecular conformation on drawing melt quenched samples. Three processes were identified: (i) crystallisation of amorphous polymer; (ii) the untwisting of crystallite ribbons perpendicular to the draw direction and in the sample plane (rotation of unit cells about the *b*-axis) and (iii) coarse slip (associated with rotation about the *a*-axis). It is worth noting, at this point, that the technique uniquely provides simultaneous information on (i) the alignment of new crystals and the arrangement of labelled stems within them; (ii) the range of deformation over which processes such as crystallisation and coarse slip occur for different materials; (iii) the deformation range for the untwisting of spherulite ribbons (in one favourable case) and (iv) perhaps most importantly, the onset and extent of crystal breakup during coarse slip. This last feature allows estimates to be made of the size of remaining crystal blocks at various stages of deformation, enabling detailed differences in the deformation process to be determined for different molecular architectures.

For both low and high molecular weights, the initial increase in *a*-polarised absorbance and decrease in *b*-polarised absorbance is related to chain crystallisation, with the corresponding alignment of chains. New or increased doublet splittings are generally associated with the newly formed

crystals. For sample LL/95/385, this process appears to be complete at a draw ratio of around 4, while for the remaining 3 samples it continues throughout the deformation range. For copolymer guest molecules, this interpretation is supported by the observation of an initial reduction in the proportion of isolated stems (Figs. 17 and 21) and again indicates a specific orientation of the new crystallites. Only a small increase in one doublet splitting was observed for sample CL/95/385, with no increase at all for sample CC/95/181, indicating that new groups of labelled stems are no larger than existing groups. However, the crystallisation was delayed to higher levels of deformation than for purely linear polymers: this is particularly noticeable for sample CC/95/181, where the *a*-polarised absorbance remains constant until a draw ratio of around 3.0 (Fig. 19). This effect was attributed to copolymer branches hindering both crystallisation and the translation of molecular chains through lamellae.

The decrease in *a*-polarised absorbance in sample LL/95/385 at draw ratios above 4 is attributed to untwisting of spherulite ribbons along radii perpendicular to the draw direction and in the sample plane. Although this behaviour is not observed for the other samples, the same process is likely to occur at the same time as continuing crystallisation. This would account for the declining change in *a*-polarised absorbance with increasing draw ratio.

The MCIRS technique is particularly informative in characterising the extent of crystallite break-up as a result of coarse slip. The presence of a minimum in the proportion of isolated stems and a coincident maximum in the proportion of small groups (Figs. 8, 17 and 21) is indicative of the onset of crystal breakup, and this is delayed to higher draw ratios for copolymer guest molecules. The increase in singlet band area, decrease in doublet area, reduction in doublet splittings and the disappearance of outermost doublets are all evidence of coarse slip. Detailed information is obtained about the evolution of group size during deformation. While the undeformed samples show significant numbers of groups containing as many as 9 labelled stems (sample LL/413/385) or 18 for sample CC/95/181, for the highest draw ratios reported here the largest remaining groups contain only 3 or 4 stems or 4–6 stems, respectively. This suggests that crystallite blocks are reduced in extent to a maximum of around 18 Å at draw ratios of around 7 for sample LL/413/385 and around 27 Å for sample CC/95/181 at a draw ratio of 5.0. There is little evidence here that the untwisting of lamellar ribbons occurs at an earlier stage than crystallite break-up. The corresponding figure for the maximum block size remaining in sample LL/95/385 at a draw ratio of around 7 is 9 and 27 Å for sample CL/95/385 at a draw ratio of 5.0.

A progressive increase in width of the central singlet component of the CD_2 bending vibration in samples LL/413/385 and CL/95/385 is tentatively attributed to variations in molecular strain, as might be experienced by tie molecules.

Acknowledgements

We are grateful to Dr Peter Barham (University of Bristol) and BP Chemicals for supplying and characterising the samples. We wish to thank BP Chemicals for supporting SC. We are indebted to Dr Warren Reed (BP Chemicals) and Dr Mary Vickers (University of Cambridge) for valuable discussions and to Dr Mike Dixon (BP Chemicals) for the loan of the Minimat tensile tester. We would also like to thank Prof. Goran Ungar (University of Sheffield) for the use of SAXS facilities.

References

[1] Li DS, Garmestani H, Alamo RG, Kalidindi SR. Polymer 2003;44:5355.
[2] Vickers ME, Fischer H. Polymer 1995;36:2667.
[3] Butler MF, Donald AM, Ryan AJ. Polymer 1997;38:5521.
[4] Hughes DJ, Mahendrasingam A, Oatway WB, Heeley EL, Martin C, Fuller W. Polymer 1997;38:6427.
[5] Coutry S, Spells SJ. Polymer 2003;44:1949.
[6] Song Y, Nitta K-H, Nemoto N. Macromolecules 2003;36:1955.
[7] Spells SJ. In: Spells SJ, editor. Characterization of solid polymers. London: Chapman & Hall; 1994.
[8] Coutry S, Spells SJ. Polymer 2002;43:4957.
[9] Okoroafor EU, Spells SJ. Polymer 1994;35:4578.
[10] Tanigami T, Cho MH, Kyu T. Eur Polym J 1995;31:671.
[11] Alamo RG, Viers BD, Mandelkern L. Macromolecules 1993;26:5740.
[12] Puig CC, Aviles MV, Joskowicz P, Diaz A. J Appl Polym Sci 2001;79:2022.
[13] Rabiej S, Goderis B, Janicki J, Mathot VBF, Koch MHJ, Groeninckx G, et al. Polymer 2004;45:8761.
[14] Coutry S. PhD Thesis, Sheffield Hallam University; 2001.
[15] Hay IL, Keller A. J Mater Sci 1967;2:538.
[16] Sasagury K, Hoshino S, Stein RS. J Appl Phys 1964;35:47.
[17] Oda T, Nomura S, Kawai H. J Polym Sci A2 1993;3:1993.
[18] Nomura S, Asanuma A, Suehiro S, Kawai H. J Polym Sci A2 1971;9:1991.
[19] Hiss R, Hobeika S, Lynn C, Strobl G. Macromolecules 1999;32:4390.
[20] Lagaron J, Dixon NM, Reed W, Pastor JM, Kip BJ. Polymer 1999;40:2569.
[21] Siesler HW. Infrared Phys. 1984;24:239.
[22] Sadler DM, Barham PJ. Polymer 1990;31:36.
[23] Pazur RJ, Ajji A, Prud'homme RE. Polymer 1993;34:4004.
[24] Glenz W, Peterlin A. In: Peterlin A, editor. Plastic deformation of polymers. New York: Marcel Dekker; 1971.
[25] McRae MA, Maddams WF, Freddy JE. J Mater Sci 1976;11:2036.
[26] Baker AME, Windle AH. Polymer 2001;42:651.
[27] Galeski A, Bartczak Z, Argon AS, Cohen RE. Macromolecules 1992;25:5705.
[28] Hay IL, Keller A. Kolloid Z 1965;204:43.
[29] Butler MF, Donald AM, Ryan AJ. Macromolecules 1995;28:6383.
[30] France C, Hendra PJ, Maddams WF, Willis HA. Polymer 1987;28:710.
[31] Alamo RG, Viers BD, Mandelkern L. Macromolecules 1993;26:5740.
[32] Gorce J-P, Spells SJ. Polymer 2002;43:4043.